AD NUMBER

AD079127

NEW LIMITATION CHANGE

TO

Approved for public release, distribution unlimited

FROM

Distribution authorized to U.S. Gov't. agencies and their contractors; Administrative/Operational Use; AUG 1955. Other requests shall be referred to Ballistic Research Laboratories, Aberdeen Proving Ground, MD.

AUTHORITY

BRL ltr dtd 22 Apr 1981

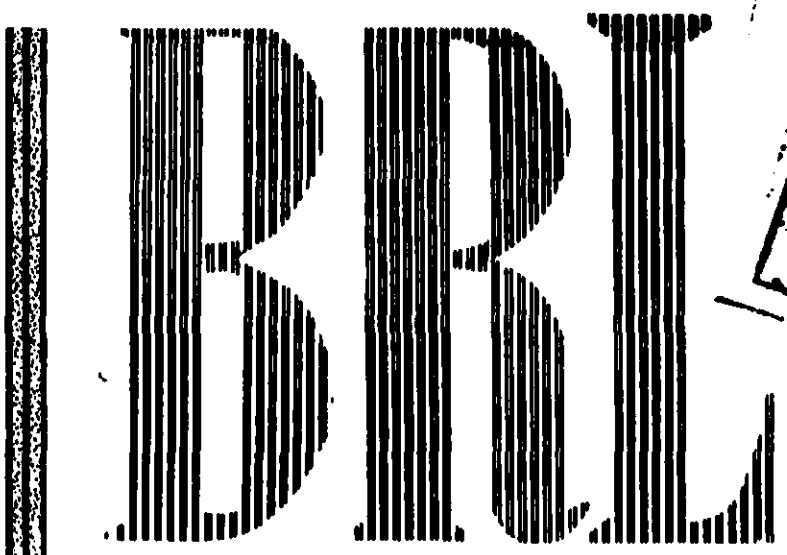

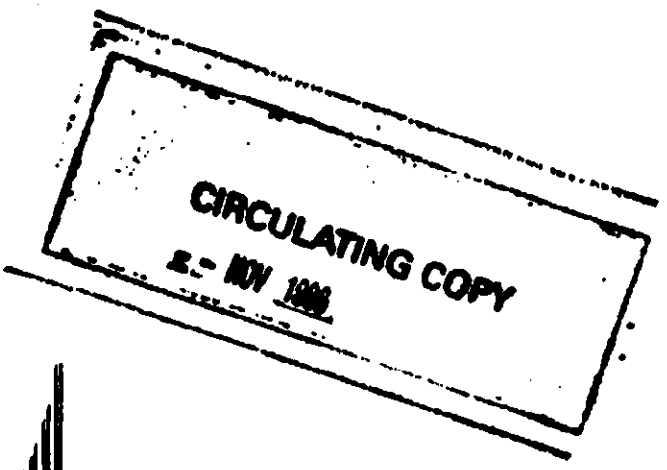


REPORT No. 946

# Refraction Of Light Traversing A Conical Shock Wave Part I: Constant Density, Application To Shadowgraphs



RAYMOND SEDNEY
NATHAN GERBER

DEPARTMENT OF THE ARMY PROJECT No. 5B03-03-001
ORDNANCE RESEARCH AND DEVELOPMENT PROJECT No. TB3-0108

BALLISTIC RESEARCH LABORATORIES

ABERDEEN PROVING GROUND, MARYLAND

B A L L I S T I C  R E S E A R C H  L A B O R A T O R I E S

REPORT NO. 946

August 1955

# REFRACTION OF LIGHT TRAVERSING A CONICAL SHOCK WAVE
## PART I: CONSTANT DENSITY, APPLICATION TO SHADOWGRAPHS

Raymond Sedney
Nathan Gerber



Department of the Army Project No. 5B03-03-001
Ordnance Research and Development Project No. TB3-0108

A B E R D E E N  P R O V I N G  G R O U N D,  M A R Y L A N D

B A L L I S T I C  R E S E A R C H  L A B O R A T O R I E S

REPORT NO. 946

RSedney/NGerber/mjs
Aberdeen Proving Ground, Md.
August 1955

# REFRACTION OF LIGHT TRAVERSING A CONICAL SHOCK WAVE
## PART I: CONSTANT DENSITY, APPLICATION TO SHADOWGRAPHS

ABSTRACT

By means of geometrical optics the refraction of light traversing a cone is investigated. It is hoped that this study will aid in the interpretation and treatment of information from shadowgraphs and interferograms used in the investigation of the axially symmetric airflow about sharp-nosed projectiles in supersonic flight.

In Part I, after the necessary formulas are derived, applications to shadowgraphs are made. (Applications to interferometry will be considered in Part II.)

A simple physical model is assumed: a cone of index of refraction $n_2$ located in a space of constant index of refraction $n_1$ ($< n_2$) with parallel light impinging on the cone perpendicular to its axis. The main reason for choosing a cone is that it has simple geometrical properties; however, many of the general ideas developed will be applicable to any rotationally symmetric shock wave. In Parts I and II a further simplification is made; $n_2$ is considered constant. (Part III will consider a variable $n_2$ appropriate to Taylor-Maccoll flow.)

With $n_2$ constant the ray tracing problem is fairly simple since no differential equations must be solved. Snell's law and some analytic geometry give the "exit functions". These designate the location and direction of light rays emerging from the cone and are used to calculate light patterns on shadowgraphs. (In Part II they are used to calculate fringe shifts.) Since considerable labor is involved in calculating them, the exit functions have been computed on the ENIAC for a wide range of cases, where the parameters are the cone angle and ratio of refractive indices.

This page Left Intentionally Blank

# I INTRODUCTION

Optical methods are used extensively for examining supersonic flows. In order to interpret the resulting photographs of the flow it is necessary to study the behavior of the light which passes through the supersonic disturbance. Several studies of the optical problems involved in this interpretation are reported in references [1], [2], [3], and [4]. Additional references may be found in [1]. In this report we shall study some of the optical problems arising in the interpretation of shadowgraphs.

In Part II refraction effects in interferograms will be considered. The schlieren method will not be considered in detail. (The shadowgraph, interferogram, and schlieren methods of examing supersonic flows can, in their gross effects, be separated. However, there are usually small effects of one method mingled with the gross effects of another. For example, a shadowgraph of a free flight projectile was taken using a small rotating mirror to stop the motion. This shadowgraph exhibited several fringes behind the shock wave and some schlieren effect where one edge of the mirror acted as a "knife edge".)

Consider the problem of light ray tracing in the supersonic conical flow field about the nose of a cone cylinder at zero yaw with an attached shock wave. We shall assume parallel light traveling perpendicular to the axis of the conical shock. The rays pass from a medium of refractive index $n_1$, through the conical region of refractive index $n_2(x,y,z)$, and into the original medium again. There they are recorded on a photographic plate placed normal to the initial beam of light, producing an interferogram or a shadowgraph according to the arrangement of the experimental apparatus.

Since the change in index of refraction, after the initial jump across the shock wave, is small for large regions of the flow field, it is not too unreasonable to take the index of refraction to be constant. This simplifies the problem of ray tracing considerably since the path will be a broken straight line. The difficulty of solving sets of differential equations is eliminated.

With the simplification of a constant index of refraction the calculations required are straightforward but still rather lengthy. One reason for this is that the problem is three-dimensional. Some additional assumptions can be introduced to reduce the problem to two dimensions as in [2]. However, some significant differences between the results of [2] and the three-dimensional treatment were found in a preliminary investigation. Hence the present study was undertaken.

From the ray tracing study reported here qualitative explanations can be obtained of some of the characteristics of shadowgraphs for large values of the parameters Mach number and free stream density. The explanations are qualitative mainly because it is necessary to consider rays other than those in a small neighborhood of the grazing ray so that the constant index assumption is not strictly justified. The calculated width of the

shadow at a shock wave agrees fairly well (twenty per cent) with measured values. Equally good agreement can be obtained by making the further assumptions necessary to reduce the problem to a two-dimensional one ( [2] , [3] ) except in some cases. These cases are those in which R/D is either very small or very large, where R is the radius of the osculating circle of [2] and D is the distance from the disturbance to the photographic plate.

## II DETERMINATION OF THE EXIT FUNCTIONS

A cone of refractive index $n_2$ is imbedded in a space of refractive index $n_1$, where $n_1 < n_2$. The half-angle of the cone is $\phi$. A beam of rays perpendicular to the axis enters the cone, is refracted, and proceeds to a photographic plate. We choose the coordinate axes so that z is the axis of the cone and the rays travel in the positive x direction ($\bar{i}, \bar{j}$, and $\bar{k}$ denoting unit vectors in the x, y, and z directions, respectively). Fig. 2.1 illustrates the coordinate system and the path of the light.

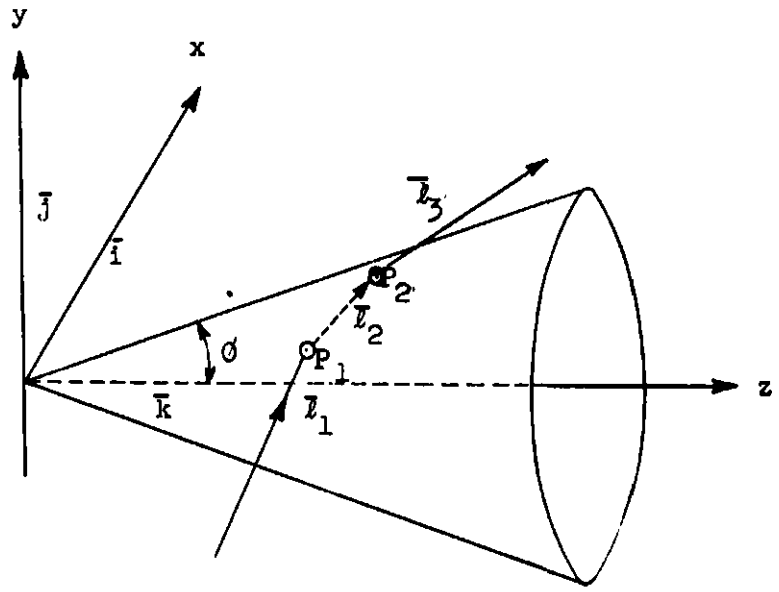


Fig. 2.1

If $\bar{r}$ denotes the position vector of a point on the cone, the equation of the cone is

$$\bar{r} \cdot \bar{k} = z = |\bar{r}| \cos \phi,$$

or in rectangular coordinates --

$$x^2 + y^2 = z^2 \tan^2 \phi \qquad (2.1)$$

Let $\bar{\rho}$ be the unit vector in the direction of $\bar{r}$ , i.e., $\bar{\rho} = \bar{r}/|\bar{r}|$. Then $\bar{\rho} \cdot \bar{k} = \cos \phi$.

The unit normal vector $\bar{N}$ at the point $\bar{r}$ lies in the plane containing $\bar{\rho}$ and $\bar{k}$. From the conditions $\bar{N} \cdot \bar{N} = 1$ and $\bar{N} \cdot \bar{\rho} = 0$ the outward unit normal is found to be

$$\bar{N} = \cot \phi \, \bar{\rho} - \csc \phi \, \bar{k} \tag{2.2}$$

At a surface of discontinuity in refractive index the refracted ray lies in the plane containing the incident ray and the normal to the surface. Fig. 2.2 illustrates the refraction of a ray with angle of incidence $\theta_1$ and angle of refraction $\theta_2$

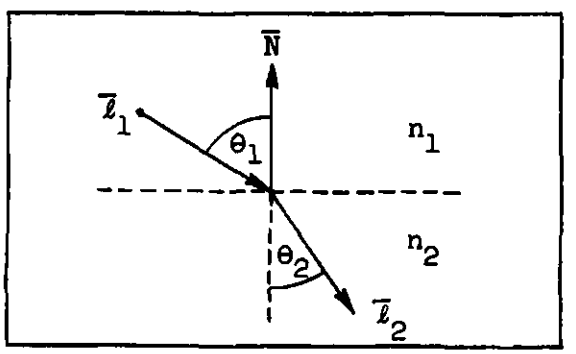


$n_2 > n_1$

Fig. 2.2

(where $\bar{\ell}_1$ is a unit vector along the incident ray and $\bar{\ell}_2$ a unit vector along the refracted ray). Snell's law states that

$$\sin \theta_2 = (n_1/n_2) \sin \theta_1 \tag{2.3}$$

Let $$p = - \bar{\ell}_1 \cdot \bar{N} = \cos \theta_1 \tag{2.4}$$

Fig. 2.3 shows the projection of the optical phenomenon in the x, y plane. We shall let $z = z_1$ be the equation of the incident plane beam of light, and we shall use p in the equations as the parameter identifying the individual rays.

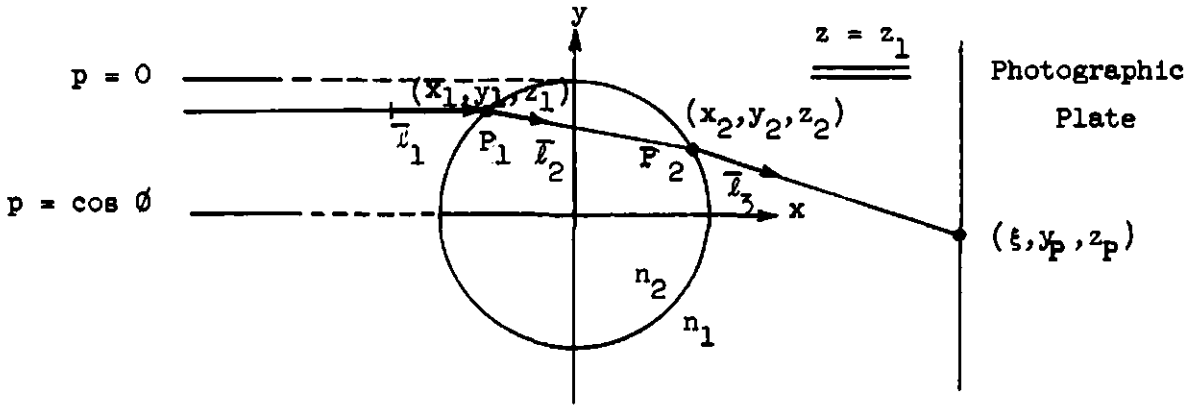


Fig. 2.3

The equation of an incident ray is $\bar{l}_1 = \bar{I}$.

From eqns. (2.2) and (2.4) $p = -\bar{l}_1 \cdot \bar{N}_1 = -\cot\phi\,(\bar{I} \cdot \bar{\rho}_1)$

Since $\bar{\rho}_1 = (x_1\bar{I} + y_1\bar{J} + z_1\bar{K})/(z_1 \sec\phi)$,

$$p = -(x_1 \cot\phi)/(z_1 \sec\phi)$$

From this equation and eqn. (2.1) we get the coordinates of $P_1$ in terms of p and $z_1$:

$$\left.\begin{aligned} x_1 &= -z_1 p \tan\phi \sec\phi \\ y_1 &= z_1 \tan\phi \sqrt{1 - p^2 \sec^2\phi} \\ z_1 &= z_1 \end{aligned}\right\} \qquad (2.5)$$

Because of the symmetry we need only study the incident rays in the upper half of the picture, though rays from the lower half will be taken into account when we consider th light pattern on the photographic plate.

As $P_1$ moves from $y_1 = z_1 \tan \phi$ (grazing ray) to $y_1 = 0$, p varies from zero to cos $\phi$.

Let $p'$ be the cosine of the angle of exit, that is, the angle that the emerging ray makes with the normal at the point $P_2$. In terms of the initial conditions $p'$ is given by*

$$(p')^2 = (1/\beta^2)\left[(\alpha - \beta p)^2 \left(\frac{\alpha^2 - \cot^2 \phi}{1 - \beta^2 + \cot^2 \phi}\right)^2 - (1 - \beta^2)\right] \quad (2.6)$$

where

$$\left.\begin{aligned} \beta &= n_1/n_2 \\ \alpha &= \beta p - \sqrt{p^2\beta^2 + (1 - \beta^2)} \end{aligned}\right\} \quad (2.7)$$

For the grazing ray p = 0, and eqn. (2.6) reduces to

$$(p')^2 = -(4/\beta^2)\left[(1 - \beta^2)^2 \cot^2 \phi\right] \Big/ (1 - \beta^2 + \cot^2 \phi)^2,$$

which shows that $p'$ is imaginary and consequently the tangential ray exceeds the critical angle upon leaving the cone. One would then expect a small bundle of rays in the neighborhood of the tangential ray to be totally reflected. (In all cases considered this bundle is so small that it has a negligible effect on the shadowgraph.)

In terms of initial conditions the coordinates of $P_2$, the point of exit, are found to be (as derived in the Appendix)

$$\left.\begin{aligned} x_2/z_1 &= (1/d)(\tan \phi \sec \phi)\left[e\beta \cot \phi - p(e\alpha \cot \phi + d)\right] \\ y_2/z_1 &= (1/d)(\tan \phi \sqrt{1 - p^2 \sec^2 \phi})\ (e\alpha \cot \phi + d) \\ z_2/z_1 &= (1/d) \end{aligned}\right\} \quad (2.8)$$

where

$$\left.\begin{aligned} d &= (\cot^2 \phi - \alpha^2) / (1 - \beta^2 + \cot^2 \phi) \\ e &= -2(\alpha - p\beta) \cot \phi / (1 - \beta^2 + \cot^2 \phi) \end{aligned}\right\} \quad (2.9)$$

The exit ray is designated by the unit vector

$$\bar{l}_j = \lambda \bar{I} + \mu \bar{j} + \nu \bar{k} \quad (2.10)$$

*See Appendix for derivation.

The direction cosines $\lambda$, $\mu$, and $\nu$ are

$$\left.\begin{aligned} \lambda &= (1/\beta)\left[\alpha' \left\{e\beta \cot \phi - p \ (e\alpha \cot \phi + d)\right\} - (p\alpha - \beta)\right] \\ \mu &= (1/\beta)\left[\cos \phi \sqrt{1 - p^2 \sec^2 \phi}\right]\left[\alpha' \ (e\alpha \cot \phi + d) + \alpha\right] \\ \nu &= (1/\beta)\left[-(\alpha + \alpha') \sin \phi\right] \end{aligned}\right\} \quad (2.11)$$

where $$\alpha' = \beta p' - \sqrt{(1 - \beta^2) + \beta^2 p'^2}, \quad (2.12)$$

taking the positive root of $p'$ in eqn. (2.6).

Eqns. (2.8) and (2.11) show that the location and direction of the rays leaving the cone can be obtained by computing a set of functions of p only, which will be applicable for any incident beam of light of the form z = constant. We shall denote $(x_2/z_1)$, $(y_2/z_1)$, and $(z_2/z_1)$ by $F_1(p)$, $F_2(p)$, and $F_3(p)$ respectively and refer to them and $\lambda$, $\mu$ and $\nu$ as exit functions.

Exit functions were calculated on the ENIAC for a series of cases (i.e., pairs of $\phi$ and $\beta$).* The combinations of $\phi$ and $\beta$ were chosen to correspond to a comprehensive range of supersonic conical flows.

## III THE SHADOWGRAPH

The image of the shock wave, defined by the undeflected grazing rays, is its projection on the photographic plate ($T_\xi$ in Fig. 3.1, which is a cross-sectional picture). Consider a refracted ray which strikes the

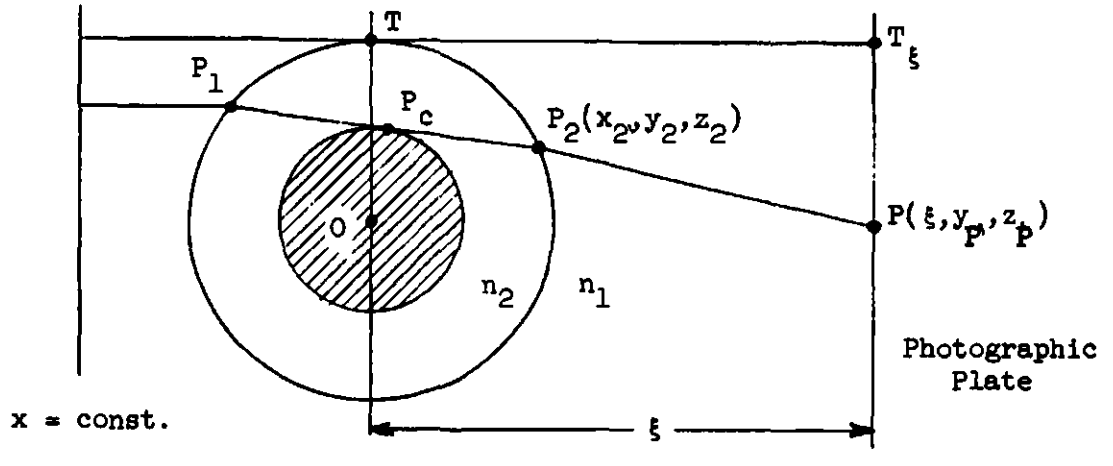


Fig. 3.1

conical shock at $P_1$. This ray leaves the cone at $P_2$ with direction cosines $\lambda$, $\mu$, $\nu$ and intersects a photographic plate located a distance $\xi$

*These functions are available in the files of the Airflow Branch, Exterior Ballistics Laboratory.

from the cone axis at the point $\xi$, $y_p$, $z_p$:

$$\left.\begin{aligned} y_p/\xi &= G_1(p)\,(z_1/\xi) + G_2(p) \\ z_p/\xi &= G_3(p)\,(z_1/\xi) + G_4(p) \end{aligned}\right\} \qquad (3.1)$$

where
$$\left.\begin{aligned} G_1 &= F_2 - (\mu/\lambda)F_1, & G_2 &= (\mu/\lambda) \\ G_3 &= F_3 - (\nu/\lambda)F_1, & G_4 &= (\nu/\lambda) \end{aligned}\right\} \qquad (3.2)$$

The functions $G_1$, $G_2$, $G_3$, and $G_4$ were calculated on the ENIAC together with the exit functions.

It is convenient to regard the optical phenomenon as a mapping of a plane x = constant, the object plane (Fig. 3.1), in the uniform beam onto the plane of the photographic plate, the image plane -- in other words, a transformation from the $z_1$, $y_1$ plane to the $z_p$, $y_p$ plane.

Equations (2.5) show that the curve in the object plane for a constant value of p is $y_1 = (z_1 \tan \phi)(1 - p^2 \sec^2 \phi)^{1/2}$, a straight line through the origin, corresponding to a plane sheet of incident rays passing through the vertex of the conical shock. Its image, from eqn. (3.1) is

$$y_p/\xi = (G_1/G_3)\,(z_p/\xi) + (G_2G_3 - G_1G_4)/G_3, \qquad (3.3)$$

a straight line also, in general not passing through the origin. In particular, if the shock is attached to a conical projectile of half angle $\theta_c$, the locus of the rays grazing the projectile is given by eqn. (3.3) for the value of p, derived in the Appendix, given by

$$p = \sec \theta_c \sqrt{\beta^2 \sin^2\phi - \sin^2\theta_c}\,/(\beta \tan \phi) = \text{constant} \qquad (3.4)$$

Hence the image of the cone is a straight line which does not intersect the image of the vertex of the shock wave, as shown in Fig. 3.2.

From the computational standpoint it is convenient to study the refraction of rays by determining the images of straight vertical beams; for moving from one beam to another then merely involves changing $z_1/\xi$ in eqn. (3.1). Fig. 3.2 presents the transforms of the upper halves of a series of $z_1$ = const. curves for one of the cases ($\phi = 44^\circ$, $\beta = .99727$; with $\theta_c = 35^\circ$)* computed by the ENIAC. From this diagram one can learn a number of characteristics of a shadowgraph.

*This case corresponds roughly to a flow of Mach number 3.2 over a cone of half angle $35^\circ$ at five atmospheres free stream pressure (Fig. 3.4).

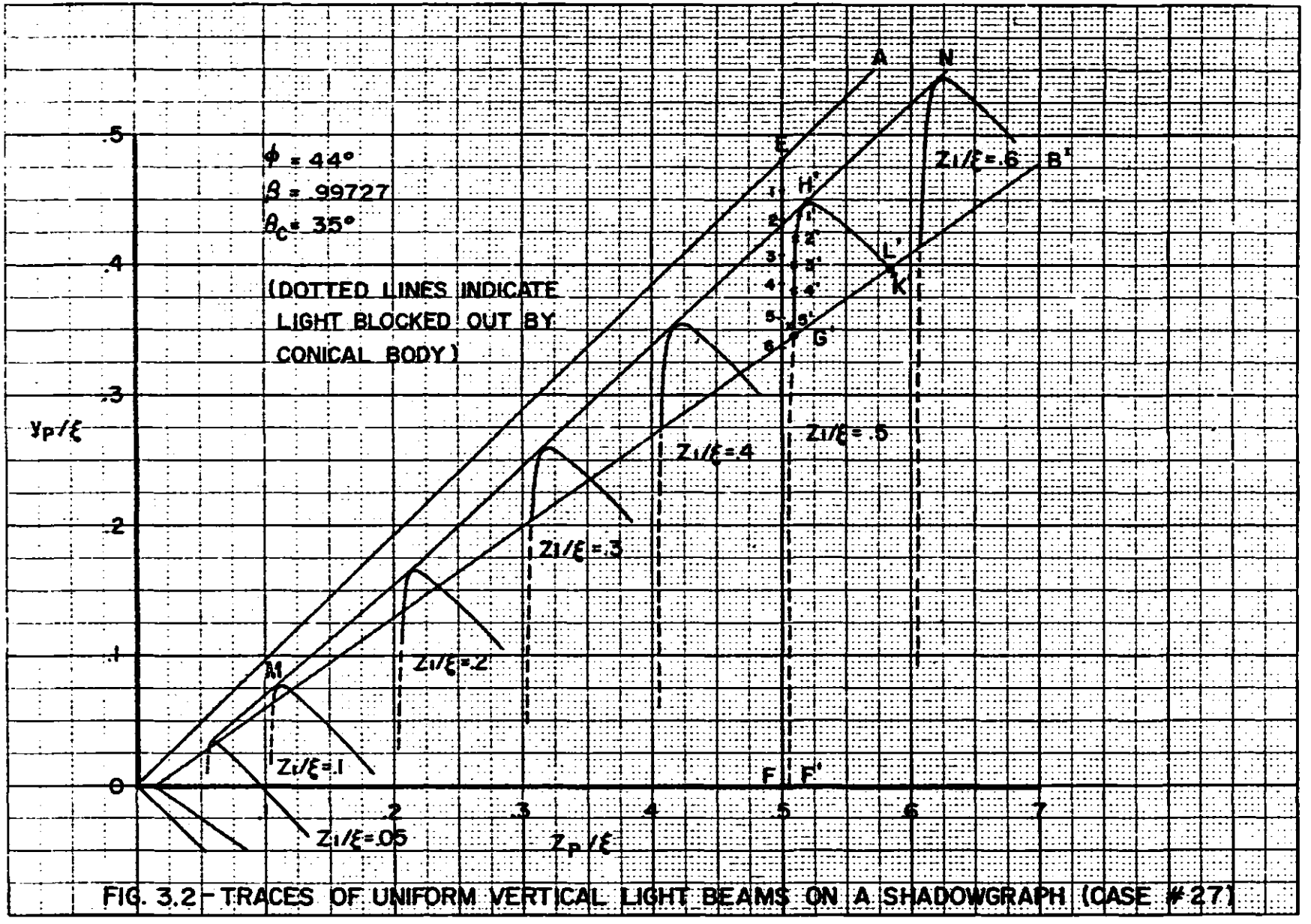


FIG. 3.2 - TRACES OF UNIFORM VERTICAL LIGHT BEAMS ON A SHADOWGRAPH (CASE #27)

Note that non-dimensional coordinates $z_p/\xi$ and $y_p/\xi$ are used. These are convenient, since the optical effects of placing the photographic plate at different distances can now be studied by means of one graph. Experimentally the plate distance can be varied by using a lens to obtain a "focused shadowgraph". Ordinarily, all the phenomena illustrated by a graph such as Fig. 3.2 are not seen on one shadowgraph. For large $\xi$ only the part of the graph for small $z_p/\xi$ is seen because the large values of $z_p/\xi$ are actually out of the conical flow region; for small $\xi$ the larger values of $z_p/\xi$ come into the picture, and compression of the picture causes loss of detail in the region of small $z_p/\xi$.

We consider a particular curve of the family, say $z_1/\xi = .5$, and designate it by $K'L'H'G'F'$. (This is in the range of larger values of $z_1/\xi$. For very small $z_1/\xi$ ($< .05$) the phenomena are somewhat different.) This curve, roughly drawn in Fig. 3.3 (b), is the image of EKGF in Fig. 3.3(a). $K'$ corresponds to K, the ray with the smallest value of p that will give a real value (namely, zero) to $p'$. As p

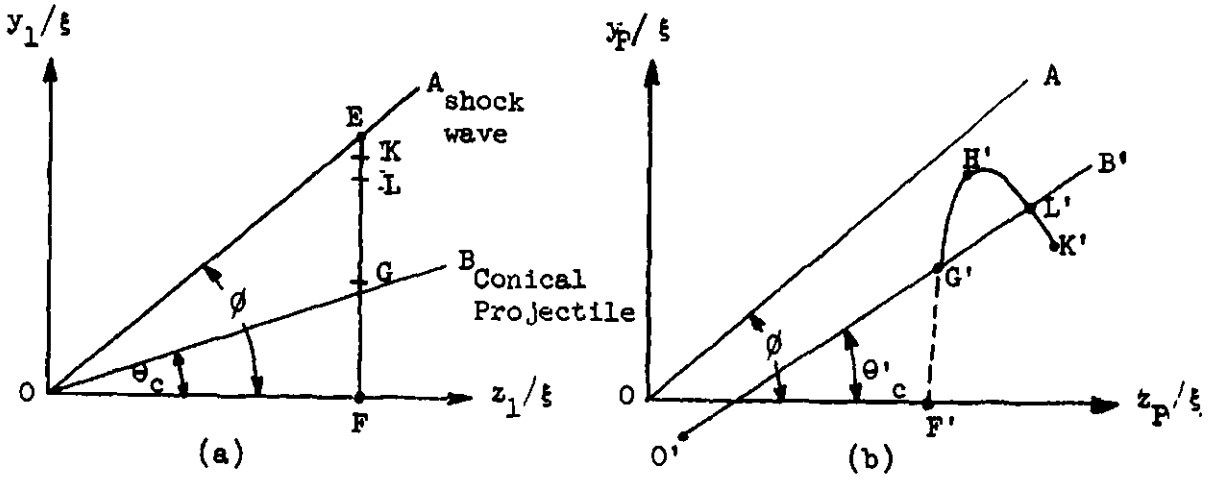


Fig. 3.3

increases (i.e., the object point moves from K to F in Fig. 3.3 (a)) the image point moves through $K'L'H'G'$. $G'$ corresponds to G, the ray which grazes the conical body. All further rays, G --- F, are blocked out by the solid cone; thus the $G'F'$ segment of light in Fig. 3.3(b) does not appear on the shadowgraph. $K'L'$ is visible, however; thus some light falls within the shadow of the projectile. This will be discussed below.

The dark space between the projection of the shock wave and the $z_1/\xi$ = const. curves is the shock wave "shadow", and its lower boundary

is the envelope of these curves (MN in Fig. 3.2). It is seen from the behavior of these curves that the inverse transformation ($y_p, z_p$ to $y_1$, $z_1$) is double valued over a large portion of the region considered and is singular along this envelope. The shock wave shadow boundary corresponds to the locus of points in the object plane for which the Jacobian $J = \partial(y_p, z_p)/\partial(y_1, z_1)$ is zero. Setting the Jacobian equal to zero yields the following relationship between $z_1$ and p:

$$z_1(p) = \xi \left(G_3 G_2' - G_1 G_4'\right) \Big/ \left[G_1^2 (G_3/G_1)'\right] ,$$

where the prime denotes differentiation with respect to p. One can then in principle calculate the boundary of the shock shadow by differentiating the G functions numerically and applying eqn. (3.1) to give the boundary curve in parametric form. However, in practice this would be a very laborious calculation. In Fig. 3.2 the inner boundary of the shadow was simply sketched in. Nevertheless, two general conclusions can be drawn to compare with the results of [2] . (i) As $z_p/\xi$ approaches zero the width of the shadow (measured perpendicular to the outer boundary) does not approach zero. Lewy's approximation in [2] gives a shadow width proportional to $z_p^{1/3}$. (The image of the tip region is discussed more fully below.) (ii) As $z_p/\xi$ increases, the shadow width increases very nearly as the one-third power of $z_p$. But eventually this decreases, becomes zero, and thereafter there is no shadow. In [2] a monotonic increase is predicted. The fact that the shadow width does not increase monotonically is not illustrated in Fig. 3.2. However, this can be seen by considering the slopes of the straight lines p = constant given by eqn. (3.3). The slope is always $G_1/G_3$, and it is found that for the first ray that emerges from the cone (and a small bundle of rays in the neighborhood of it) $G_1/G_3$ is always greater than tan $\phi$. Hence eventually this bundle of rays is imaged outside of the true shock wave. Thus for $z_p/\xi$ (or R/D in the notation of [2] ) small and large the approximations of [2] are not valid.

Practically, to have a large enough $z_p/\xi$ for a zero shadow width it would be necessary to have a very small $\xi$ obtained by focusing on a plane inside the disturbance. In fact this would be closely realized in taking an interferogram where the plane of focus is slightly off the median plane. A note of caution in interpreting Fig. 3.4: the zero shadow width where the shock begins to curve is not related to the above discussion. This arises because of the expansion fan from the shoulder, and is discussed in [3] .

Further information can be obtained from a study of the illumination of the shadowgraph. Let $I_1$ be the illumination per unit area (assumed constant) in the beam before entering the disturbance, and $I_p$ ($y_p$, $z_p$)

th illunination per unit area on the photographic plate. If light from the area $dy_1 \cdot dz_1$ illuminates the area $dy_p \cdot dz_p$ on the plate, then

$$I_p dy_p dz_p = I_1 \, dy_1 \, dz_1 = I_1 \left[ \partial(y_1, z_1)/\partial(y_p, z_p) \right] \, dy_p \, dz_p$$

Hence $$I_p = I_1 \left[ \partial(y_1, z_1)/\partial(y_p, z_p) \right] = I_1 \, J',$$

where $J'$ is the Jacobian of the transformation $y_p$, $z_p$ to $y_1$, $z_1$. Actually we should sum two Jacobians to account for the fact that this transformation is double valued. This addition should take account of the phase difference also. However, we shall not examine the interference effect here.

Since, as we have just seen, the Jacobian $J = 1/J'$ is zero at the boundary of the shock shadow, geometrical optics predicts infinite intensity just behind the shock wave on the shadowgraph. Although this condition is not realized in actuality, the intensity of the illumination in this region is very high.

By locating the images of a series of rays equally spaced on an initial beam of light, one can obtain an idea of the distribution of light on the shadowgraph. Thus, e.g., rays 1, 2, 3, etc. on EF in Fig. 3.2 are taken at intervals of 1/20 th of the affected beam (i.e., 1/20 th of EF = $(z_1 \tan \phi)/\xi$). Their images are points $1'$, $2'$, $3'$, etc. on $K'L'H'F'$. It is seen that about three-fourths of the light is blocked out by the conical body. Only about one-fifth of the remaining light illuminates the segment $K'L'H'$; and since most of this light must be concentrated near the shock, most of $K'L'$ (rays for small values of p) receives very little light. Thus one would still expect the conical body to be imaged sharply, although a small amount of light does enter its shadow. Furthermore, interference fringes due to optical path length differences between the corresponding rays of two beams will be noticeable only where both beams have comparable intensities, namely, near the shadow of the shock wave. It can be seen from Fig. 3.2 that for $z_1/\xi \leq .05$ light from the upper half of a beam is imaged in the lower half of the picture. Since most of the image curve corresponds to a very small fraction of the length of the beam, the illumination in the lower half of the picture due to rays from the upper half of the initial beam can in large part be neglected.

The quantity $\xi$ determines the portion of the non-dimensional picture (Fig. 3.2) which is applicable to a given shadowgraph. Thus for a range of very small $z_1/\xi$ a somewhat unusual picture is obtained. The shadowgraph shown in Fig. 3.4 ($\theta_c = 35^\circ$, $\phi \cong 44^\circ$, Mach no. $\cong$ 3.2 at 5 atm.) involves conical flow only to about $z_1/\xi = .024$, and Fig. 3.5 shows the

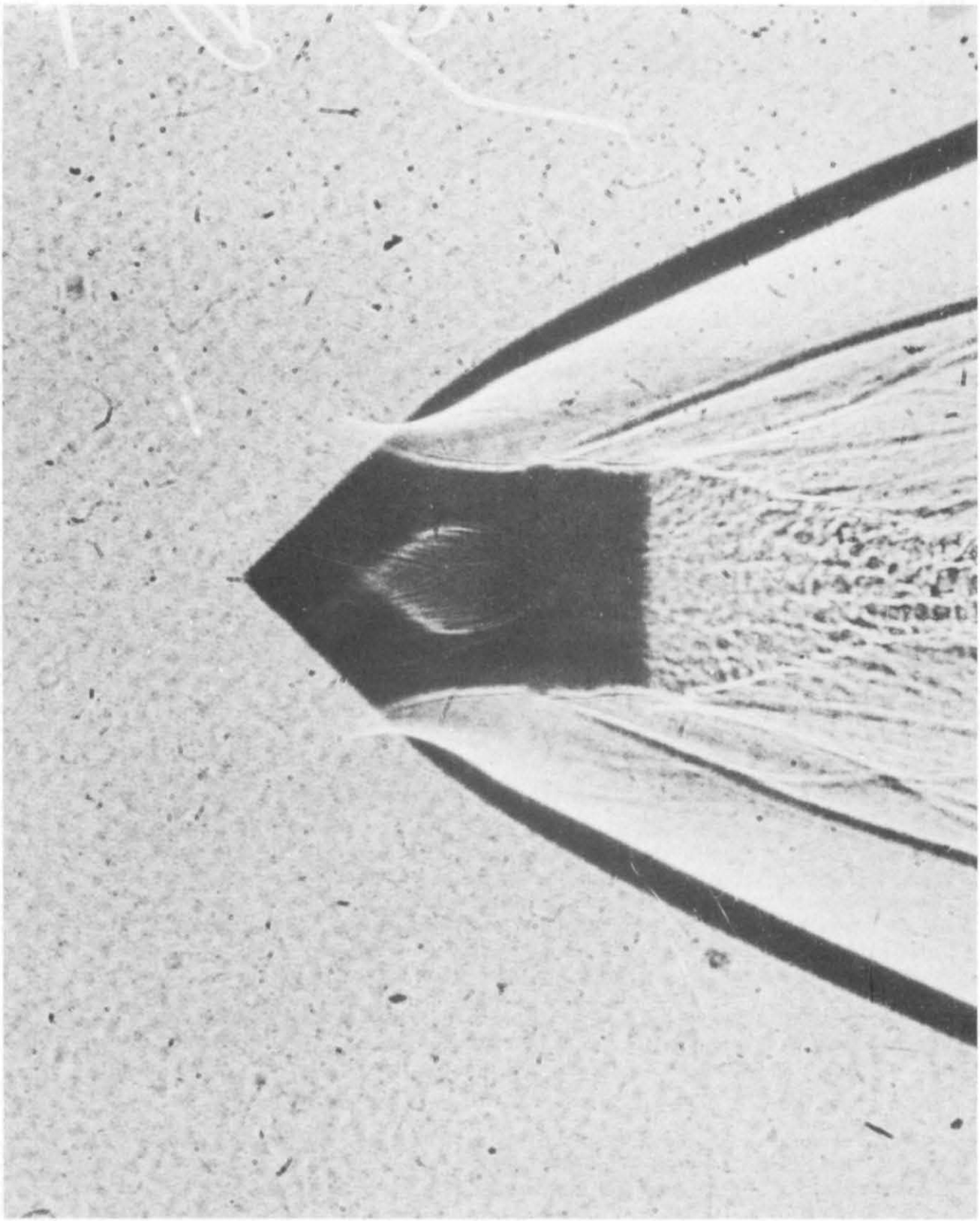

Figure 3.4

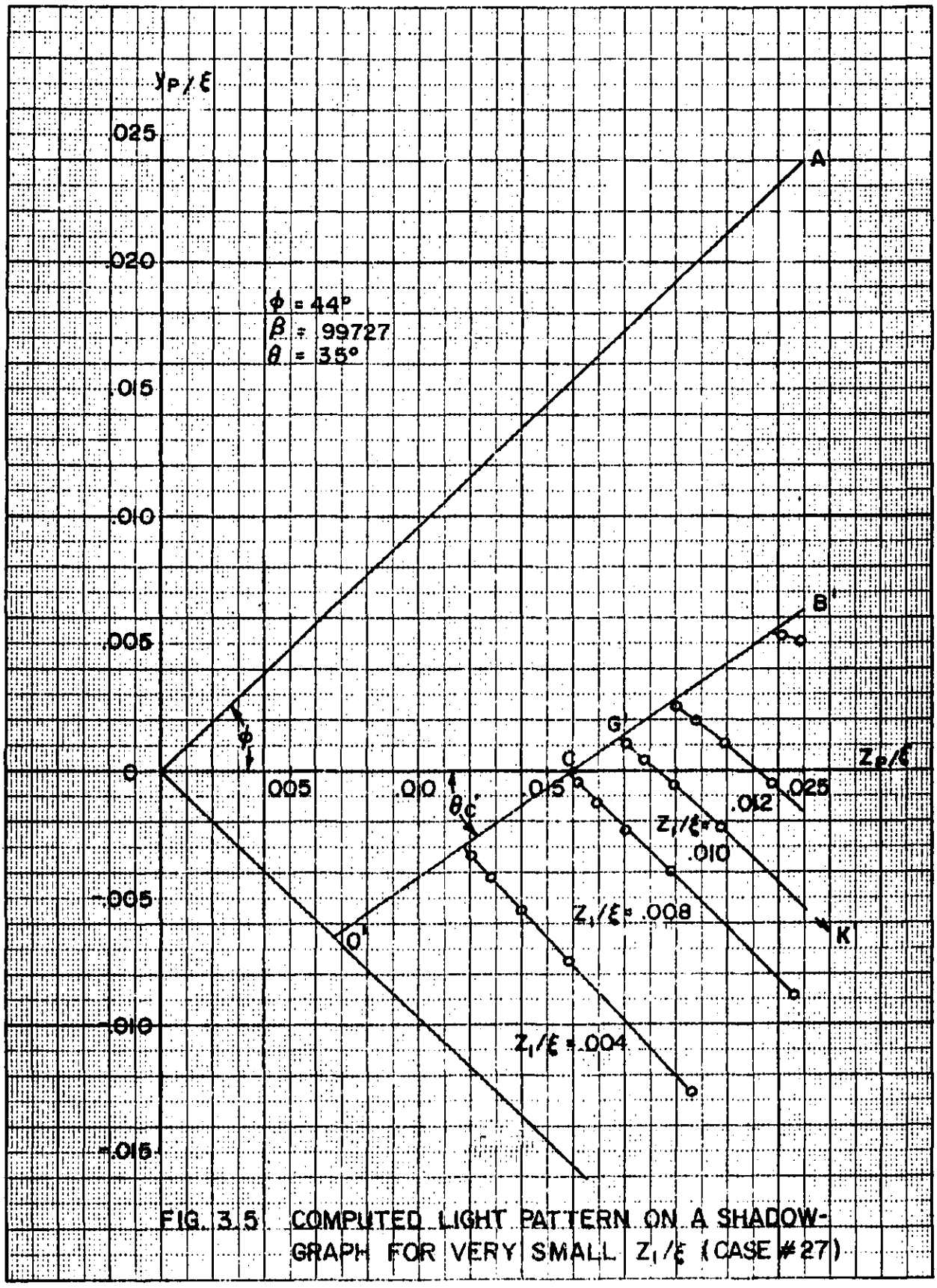


FIG. 3.5 COMPUTED LIGHT PATTERN ON A SHADOW-GRAPH FOR VERY SMALL $Z_1/\xi$ (CASE #27)

light pattern computed for an approximation to this case. Only the light from the upper rays ($y_1 > 0$) which falls on the screen is shown. The small circles represent the transforms of equally spaced points on the $z_1$ = const. lines. The shock wave shadow by itself is not visible here. This shadow coalesces with the shadow of the conical body, and the line $O'B'$ outlined by the light is the image of the conical body. Since a very small segment of the vertical light beam falls within the shadow, and the brightest portion is cut off by the conical body, the illumination is small. Light can also be observed along O C ahead of point C, the point of intersection of the cone shadow with the $z_p/\xi$ axis. The same light pattern with $y_p$ replaced by minus $y_p$ is produced on the photographic plate by the $y_1 < 0$ rays.

Thus the image of the boundary of the conical body is outlined by light rather than the absence of light and the nose of the body is imaged into two nappes of a cone. These conclusions are illustrated in Fig. 3.3. The second nappe is just barely visible because of the small illumination as discussed above. (The measured and the computed values of OC (Fig. 3.5) differ by about fifteen per cent.)

This "inversion" of the image caused by the shadows coalescing and the large deviation of rays near the tangential ray is in general verified by the shadowgraph, Fig. 3.4. However, the illuminated region inside the shadow of the projectile is not of uniform intensity; there are alternate light and dark bands. The following explanation is offered for this phenomenon: A small roughness along the conical body will produce a weak curved shock wave. This will be imaged into a dark band followed by a bright band. One side of the image can be calculated by a means of eq. (3.1). The procedure is very similar to that for finding the image of the conical body. One simply finds the set of rays which graze the wavelet (weak shock) surface. This gives a relationship between p and $z_1$, and the image curve is then given parametrically by eq. (3.1). In order to get the other side of the image, the rays which penetrate the wavelet surface would have to be considered. It does not seem necessary to consider this further complication.

For simplicity, the wavelet surface was taken to be a cone (straight shock wave) forming a Mach angle with the velocity vector at the intersection with the main shock wave. This surface depends on the parameters a and $\psi$, where a is the z coordinate of the vertex and $\psi$ is the half-angle (i.e., $x^2 + y^2 = \{z-a\}^2 \tan^2\psi$). The set of rays which grazes this surface is given by

$$z_1/a = \left[-C_2 + \sqrt{C_2^2 - C_1 C_3}\right]\Big/ C_1 \qquad (3.5)$$

where

$$C_1 = \sec^2 \phi \left[ p^2 \beta^2 \tan^2 \phi - \beta^2 \sin^2 \phi \sec^2 \psi + \tan^2 \psi \right]$$

$$C_2 = \tan^2 \psi \left[ \alpha \beta p \tan^2 \phi - 1 \right]$$

$$C_3 = \tan^2 \psi \left[ \alpha^2 \cos^2 \phi \sec^2 \psi + 1 - \alpha^2 \right]$$

The relation (3.5) between $z_1$ and p comes from solving a quadratic equation, the minus sign being ignored since this would give the rays which graze the upstream nappe of the cone.

The image was calculated for the conditions of case no. 27 ($\phi = 44^\circ$, $\beta = .99727$), with $\psi = 61^\circ\ 35'$ and various positions of the wavelet. Th s are shown in Fig. 3.6 for $a/\xi = .01, .015, .02, .03$. As previously remarked, the conical flow region extends only up to about $z/\xi = .024$ in the comparison of case no. 27 with Fig. 3.4. Thus only the first three values of $a/\xi$ are applicable, and the wavelet images agree qualitatively with Fig. 3.4. The dotted curve, labeled "envelope", is the inner boundary of the main shock wave shadow, which is very bright. Fig. 3.4 confirms the conclusion that only a small portion of this bright region is visible. Actually, on the basis of a constant index of refraction, we can calculate only one image, since getting a second image requires knowledge of rays that have passed through a wavelet. However, since the discontinuity in index of refraction across a wavelet is small, this can be neglected in calculating the images of other wavelets. Fig. 3.7 is a shadowgraph taken under different conditions (M=2.52, $\phi$=35°, 5 atm. free-stream pressure) from those of 3.4; it is included because the phenomena discussed above are more noticeable.

In Fig. 3.6 for $a/\xi = .03$ the wavelet image starts on the image of the conical body and bends around back into the body. This is to be expected for the larger values of $z_1/\xi$ (smaller $\xi$). However, it would be difficult to observe this bending back because the wavelet image would become practically invisible when it is near the bright region of the envelope.

Another application of the calculations reported here lies in estimating the "schlieren effect" on shadowgraphs and interferograms which are taken by means of a rotating mirror placed at the focus of the camera lens. The "schlieren effect" arises because some of the refracted light is deviated so far from parallelism that it is not focused on the mirror. In an interferogram this causes the fringes to b "washed out" in some regions. One can use the calculated deviations to determine the minimum size mirror which reduces the schlieren effect enough so that good quality fringes are obtained.

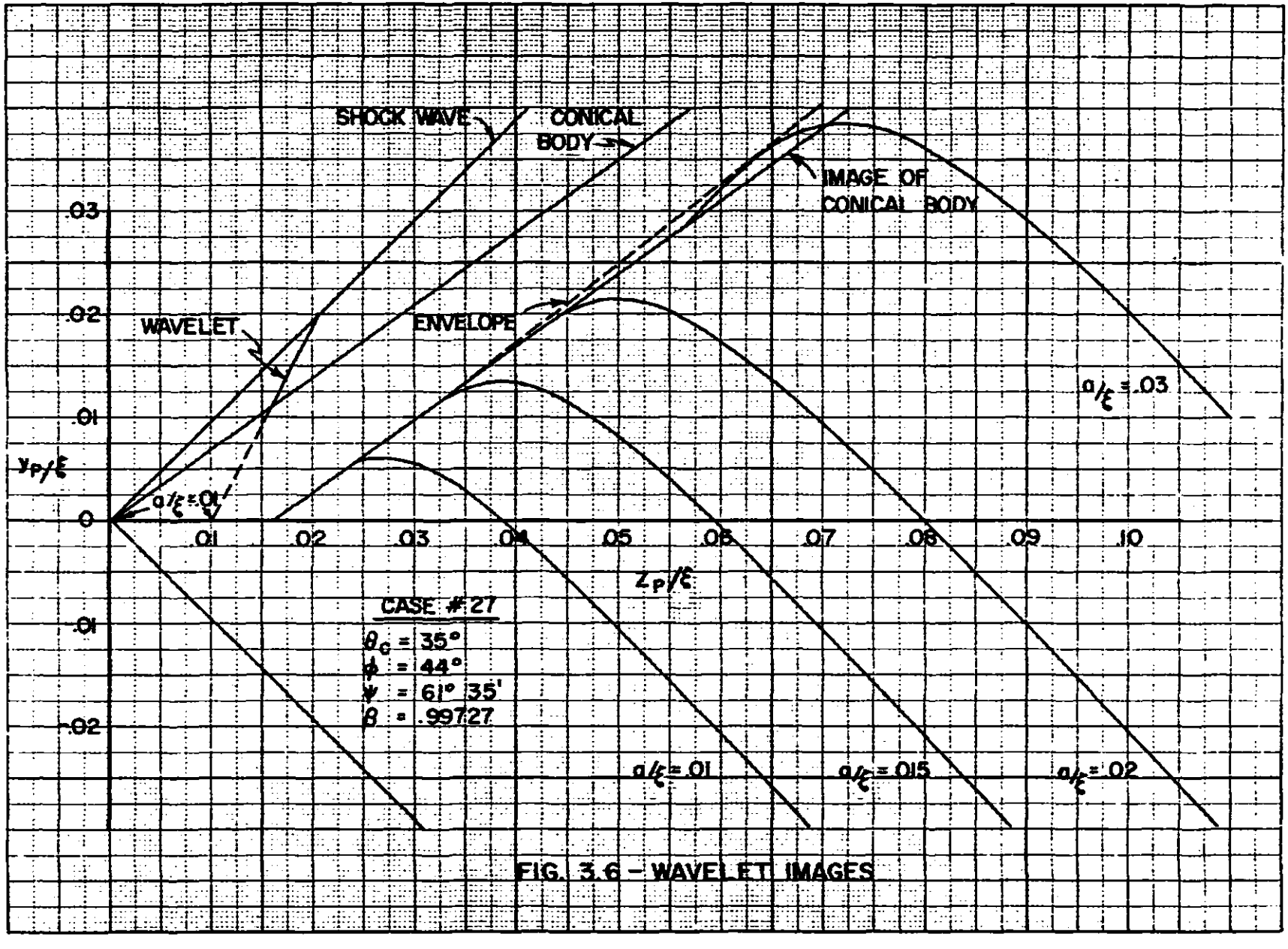


FIG. 3.6 – WAVELET IMAGES

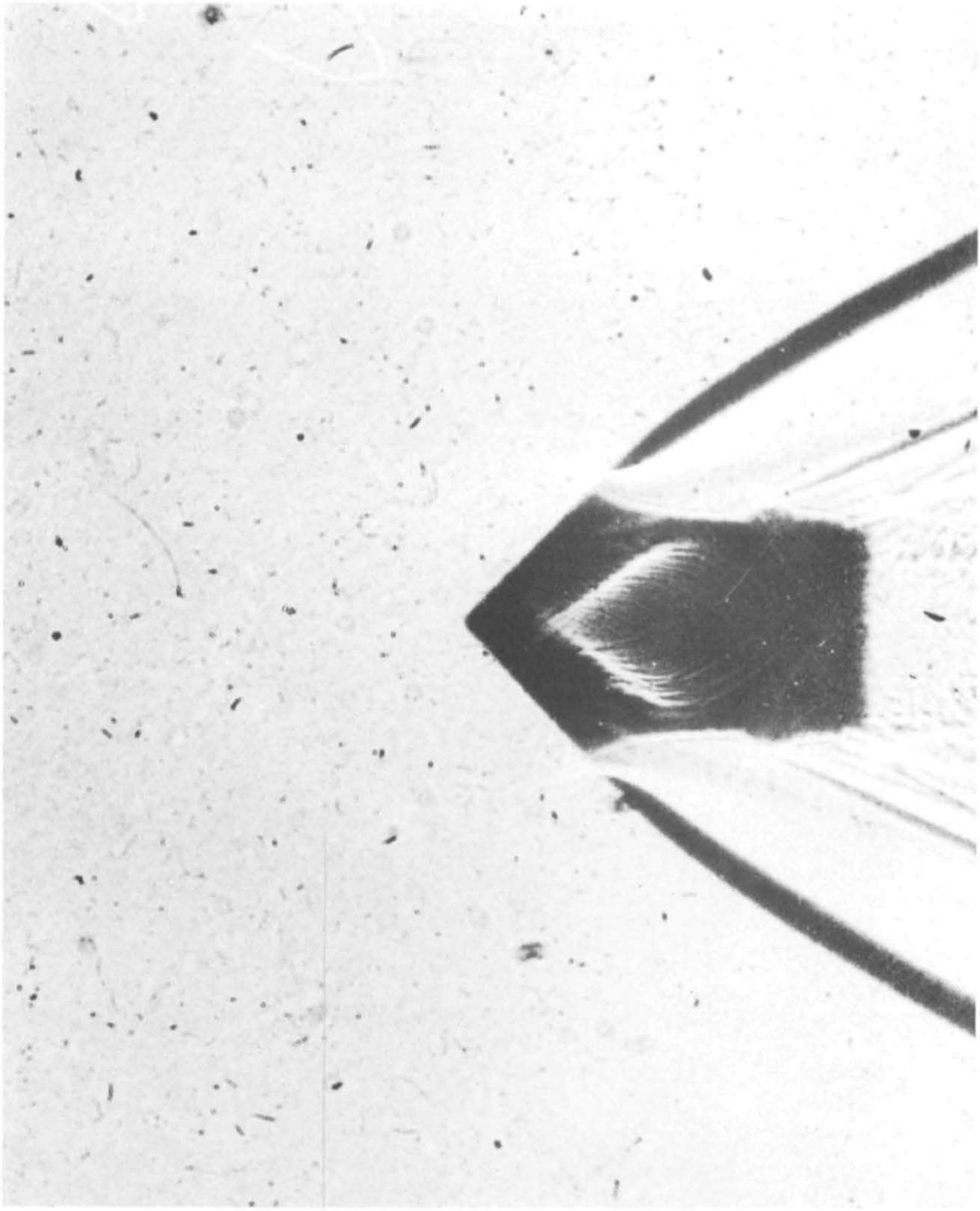

Figure 3.7



ARMY---OS---ABERDEEN PROVING GROUND, MD

ACKNOWLEDGEMENTS

The authors wish to express their appreciation to Miss Joan Bartos for assisting with the computations and graphs; Mr. George Kahl and associates for providing the shadowgraphs of Figs. 3.4 and 3.7; and Mrs. Winifred Jonas for coding and performing the ENIAC computations.

Raymond Sedney
RAYMOND SEDNEY

Nathan Gerber
NATHAN GERBER

## REFERENCES


1. Physical Measurements in Gas Dynamics and Combustion, Vol. IX, High Speed Aerodynamics and Jet Propulsion, Articles A-1, A-2, and A-3, Princeton University Press, Princeton, N. J. (1954).

2. Lewy, H., On the Relation Between the Velocity of a Shock Wave and the Width of the Light Gap It Leaves on the Photographic Plate, BRL Report 373 (1943).

3. Sedney, R., Gerber, N., Determination of Density Gradients Near Shock Waves from Shadowgraphs, BRL Report 920 (1954).

4. Hyman, M., Deflection of Light Rays in Passing Through Conical Shock Wave Patterns, Naval Ordnance Laboratory, (U. S. Naval Gun Factory), Memo. 9303.

## APPENDIX-DERIVATION OF EXIT FUNCTIONS AND SHADOWGRAPH EQUATIONS

A unit vector along the refracted ray inside the cone, $\bar{\ell}_2$, has the form (see Fig. 2.2)

$$\bar{\ell}_2 = \alpha \bar{N}_1 + \beta \bar{\ell}_1 , \tag{A-1}$$

wher $\alpha$ and $\beta$ are constants determined from eqns. (2.3) and (2.4), and the conditions:

$$\bar{\ell}_2 \cdot \bar{\ell}_2 = 1, \qquad \bar{\ell}_2 \cdot \bar{N}_1 = - \cos \theta_2$$

The result is $\beta = n_1/n_2$ and

$$\alpha = \beta p - \sqrt{\beta^2 p^2 + (1 - \beta^2)} \tag{A-2}$$

With eqns. (2.2), and (2.5), and (A-1), and the relation $\bar{\ell}_1 = \bar{i}$ one can xpress $\bar{\ell}_2$ in terms of its cartesian components:

$$\bar{\ell}_2 = (\beta - \alpha p)\bar{i} + (\alpha \cos \phi \sqrt{1 - p^2 \sec^2 \phi})\bar{j} - (\alpha \sin \phi)\bar{k} \tag{A-3}$$

The refracted ray strikes the cone at $P_2$ (see Fig. 2.3) with position vector $\bar{r}_2$ and normal $\bar{N}_2$. Since $\bar{r}_2$, $\bar{r}_1$, and $\bar{\ell}_2$ are coplanar, $\bar{\rho}_2$ $(= \bar{r}_2/|\bar{r}_2|)$ can be written

$$\bar{\rho}_2 = d\bar{\rho}_1 + e\bar{\ell}_2 \tag{A-4}$$

where d and e are the constants defined in eqn. (2.9) and determined from the following conditions:

$$\bar{\rho}_2 \cdot \bar{\rho}_2 = 1, \qquad \bar{\ell}_1 \cdot \bar{k} = 0$$

$$\bar{\rho}_2 \cdot \bar{k} = \cos \phi, \qquad \bar{\ell}_2 \cdot \bar{k} = \alpha \bar{N} \cdot \bar{k} = - \alpha \sin \phi$$

Since $|\bar{r}_1| = z_1 \sec \phi$ and $|\bar{r}_2| = z_2 \sec \phi$ it can be shown, using eqn. (A-4), that $z_2/z_1 = 1/d$ and

$$\bar{r}_2 = \bar{r}_1 + (e\, z_1 \sec \phi/d)\, \bar{\ell}_2 \tag{A-5}$$

From eqns. (2.5), (A-3), and (A-5) we determine $F_1$, $F_2$, and $F_3$, the exit functions listed in eqn. (2.8).

If a ray proceeds from a region of $n_2$ to a region of $n_1$ where $n_2 > n_1$, eqn. (A-1) will give the final ray here also. For this simply replace $\bar{\ell}_2$ by $(-\bar{\ell}_2)$ and $\bar{\ell}_1$ by $(-\bar{\ell}_1)$, and solve for $\bar{\ell}_1$.

$$\bar{\ell}_1 = (1/\beta)\ (\alpha'\ \bar{N}_1 + \bar{\ell}_2)$$

where $\alpha'$ has the same form as $\alpha$, but with a new value of p, say p'. In particular, consider the point $P_2$ (Fig. 2.3) and let $\bar{\ell}_2$ describe the ray in $n_2$ and $\bar{\ell}_3$ that in $n_1$. Then

$$\bar{\ell}_3 = (1/\beta)\ (\alpha'\ \bar{N}_2 + \bar{\ell}_2) \qquad \text{(A-6)}$$

where
$$\alpha' = \beta\ p' - \sqrt{1 - \beta^2 + \beta^2\ p'^2} \qquad \text{(A-7)}$$

and
$$p' = \bar{\ell}_3 \cdot \bar{N}_2; \qquad \text{(A-8)}$$

i.e., p' is the cosine of the angle between the emerging ray and the normal to the cone at the point of exit. $\bar{N}_2$ is obtained from eqn. (2.2).

$$\bar{N}_2 = \cot \phi\ \bar{\rho}_2 - \csc \phi\ \bar{k} \qquad \text{(A-9)}$$

From eqns. (A-6), (A-7), (A-8), and (A-9) ---

$$\beta \bar{\ell}_3 \cdot \bar{N}_2 = \alpha' + \bar{\ell}_2 \cdot \bar{N}_2$$

$$(\beta\ p' - \alpha') = \bar{\ell}_2 \cdot \bar{N}_2 = \cot \phi\ \bar{\ell}_2 \cdot \bar{\rho}_2 - \csc \phi\ \bar{\ell}_2 \cdot \bar{k}$$

$$\sqrt{(1 - \beta^2) + \beta^2\ p'^2} = \cot \phi\ \bar{\ell}_2 \cdot \bar{\rho}_2 - \csc \phi\ \bar{\ell}_2 \cdot \bar{k}$$

From eqns. (A-1), (A-3), and (A-4) ---

$$\sqrt{1 - \beta^2 + \beta^2\ p'^2} = \cot \phi\ \bar{\ell}_2 \cdot (d\bar{\rho}_1 + e\bar{\ell}_2) - \csc \phi\ (-\alpha \sin \phi)$$

$$= d \cot \phi\ (\bar{\ell}_2 \cdot \bar{\rho}_1) + e \cot \phi + \alpha$$

$$= (\alpha + e \cot \phi) + d \cot \phi\ (\alpha \bar{N}_1 \cdot \bar{\rho}_1 + \beta \bar{\ell}_1 \cdot \bar{\rho}_1)$$

$$= (\alpha + e \cot \phi) + \beta d \cot \phi\ (\bar{\ell}_1 \cdot \bar{\rho}_1)$$

Since $\bar{\ell}_1 \cdot \bar{\rho}_1 = \bar{I} \cdot \left[-(z_1\ p \tan \phi \sec \phi)\ \bar{I} + y_1 \bar{J} + z_1 \bar{k}\right] / (z_1 \sec \phi) =$

$$= -\ p \tan \phi,$$

then
$$\beta^2 p'^2 = \left[(\alpha + e \cot \phi) - \beta dp\right]^2 - (1 - \beta^2)$$

This last relation yields eqn. (2.6); then $\alpha'$ is determined from eqn. (A-7). $\bar{N}_2$ can be obtained in cartesian form from eqn. (A-9) by applying eqns. (A-4), (2.5), and (A-3):

$$\bar{N}_2 = \left[- pd + e(\beta - \alpha p)\cot\phi\right]\bar{i} + \left[(d + e\alpha\cot\phi)\cos\phi \cdot \sqrt{1 - p^2\sec^2\phi}\right]\bar{j} + \left[d\cot\phi\cos\phi - e\alpha\sin\phi\cot\phi - \csc\phi\right]\bar{k}$$

From eqn. (A-6) we then obtain the direction cosines of the emerging ray listed in eqn. (2.11).

The equation of the line $P_2P$ in Fig. 3.1 is

$$(\xi - x_2)/\lambda = (y_P - y_2)/\mu = (z_P - z_2)/\nu,$$

where $\lambda$, $\mu$, $\nu$ are given in eqn. (2.11). Remembering that $F_1 = x_2/z_1$, $F_2 = y_2/z_1$, $F_3 = z_2/z_1$, one then obtains eqn. (3.1).

For a shock wave attached to a cone of half angle $\theta_c$, the first step in determining the image of the cone is locating the intersection of the light rays with the cone. The equation of the refracted ray within the shock can be expressed, using eqn. (A-3), in terms of the parameter s as follows:

$$\left.\begin{aligned} x &= x_1 + (\beta - \alpha p)\, s \\ y &= y_1 + (\alpha\cos\phi\sqrt{1 - p^2\sec^2\phi})\, s \\ z &= z_1 - (\alpha\sin\phi)\, s \end{aligned}\right\} \qquad \text{(A-10)}$$

To find the intersection with the cone set x, y, z equal to $x_c$, $y_c$, $z_c$ respectively and apply the equation of a cone, namely:

$$x_c^2 + y_c^2 = z_c^2\tan^2\theta_c$$

This leads to the quadratic equation in s

$$As^2 + Bs + C = 0 \qquad \text{(A-11)}$$

where

$$\left.\begin{aligned} A &= 1 - \alpha^2\sin^2\phi\sec^2\theta_c \\ B &= 2z_1\sin\phi\,(\alpha\sec^2\theta_c - p\beta\sec^2\phi) \\ C &= z_1^2\,(\tan^2\phi - \tan^2\theta_c) \end{aligned}\right\}$$

The condition for the tangent ray is the requirement that eqn. (A-11) have only one solution for s; i.e., $B^2 - 4AC = 0$. This then yields eqn. (3.4).

DISTRIBUTION LIST

| No. of Copies | Organization |
|---|---|
| | Chief of Ordnance<br>Department of the Army<br>Washington 25, D. C.<br>Attn: ORDTB - Bal Sec |
| 10 | British Joint Services Mission<br>1800 K Street, N. W.<br>Washington 6, D. C.<br>Attn: Mr. John Izzard, Reports Officer |
| 4 | Canadian Army Staff<br>2450 Massachusetts Avenue<br>Washington 8, D. C. |
| 3 | Chief, Bureau of Ordnance<br>Department of the Navy<br>Washington 25, D. C.<br>Attn: Re3 Re O |
| 2 | Commander<br>Naval Proving Ground<br>Dahlgren, Virginia |
| 2 | Commander<br>Naval Ordnance Laboratory<br>White Oak<br>Silver Spring 19, Maryland<br>Of Interest to: Dr. Albert May |
| 1 | Commander<br>Naval Ordnance Test Station<br>China Lake, California<br>Attn: Technical Library |
| 1 | Commander<br>Naval Postgraduate School<br>Monterey, California |
| 4 | Commander<br>Wright Air Development Center<br>Wright-Patterson Air Force Base, Ohio<br>Attn: WCRR |
| 1 | Director<br>Air University [redacted]<br>Maxwell Air Force Base, Alabama<br>Attn: Air University Library |
| 3 | National Advisory Committee for Aeronautics<br>1512 H Street, N. W.<br>Washington 25, D. C. |
| 1 | National Advisory Committee for Aeronautics<br>Lewis Flight Propulsion Laboratory<br>Cleveland Airport<br>Cleveland, Ohio |
| 2 | National Advisory Committee for Aeronautics<br>Ames Laboratory<br>Moffett Field, California<br>Attn: Mr. V. J. Stevens<br>Mr. Harvey All n |
| 1 | National Advisory Committee for Aeronautics<br>Langley Memorial Aeronautical Laboratory<br>Langley Field, Virginia |
| 5 | Director<br>Armed Services Technical Information Agency<br>Documents Service Cent r<br>Knott Building<br>Dayton 2, Ohio<br>Attn: DSC - SA SD |
| 1 | Director<br>JPL Ordnance Corps Installation<br>Department of the Army<br>4800 Oak Grove Drive<br>Pasadena 2, California<br>Attn: Prof. H. W. Liepmann<br>Prof. H. T. Nagamatsu |

DISTRIBUTION LIST

| No. of Copies | Organization |
|---|---|
| | Commanding Officer<br>Diamond Ordnance Fuze Laboratory<br>Connecticut Avenue and Van Ness Street, N. W.<br>Washington 25, D. C.<br>Of Interest to: Dr. Irvine C. Gardner<br>Dr. L. Marton |
| 2 | Applied Physics Laboratory<br>8621 Georgia Avenue<br>Silver Spring, Maryland |
| 1 | American Optical Company<br>14 Mechanic Street<br>Southbridge, Massachusetts |
| 1 | Bausch and Lomb Optical Company<br>262 St. Paul Street<br>Rochester 2, New York |
| 1 | Brown University<br>Division of Applied Mathematics<br>Providence 12, Rhode Island<br>Attn: Professor R. F. Probstein |
| 1 | California Institute of Technology<br>Guggenheim Aeronautical Laboratory<br>Pasadena, California<br>Attn: Professor L. Lees |
| 1 | Cornell Aeronautical Laboratory<br>4455 Genesee Street<br>Buffalo 5, New York<br>Attn: Miss Elma Evans |
| 1 | Eastman Kodak Research Laboratory<br>Rochester 13, New York<br>Attn: Mr. M. Herzberger |
| 1 | Farrand Optical Company<br>Bronx Blvd. and 238 Street<br>New York 70, New York |
| 1 | Massachusetts Institute of Technology<br>Department Mechanical Engineering<br>Cambridge 39, Massachusetts<br>Attn: Professor A. H. Shapiro |
| 2 | James Forrestal Research Center<br>Princeton University<br>Princeton, New Jersey<br>Of Interest to: Prof. S. Bogdonoff |
| 1 | Massachusetts Institute of Technology<br>Gas Turbine Laboratory<br>Cambridge 39, Massachusetts<br>Attn: Prof. Ernest Neumann |
| 1 | North American Aviation, Inc.<br>Aerophysics Laboratory<br>Los Angeles 45, California |
| 1 | Lehigh University<br>Department of Physics<br>Bethlehem, Pennsylvania<br>Attn: Prof. R. J. Emrich |
| 1 | Perkin-Elmer Corporation<br>345 Hope Street<br>Glenbrook, Connecticut<br>Attn: Mr. J. Baker |
| 1 | Polaroid Corporation<br>Cambridge 39, Massachusetts<br>Attn: Mr. David Grey |
| 1 | Purdue University<br>Department of Mechanical Engineering<br>Lafayette, Indiana<br>Attn: Mr. Vollmer E. Bergdolt<br>Prof. R. C. Binder |

DISTRIBUTION LIST

| No. of Copies | Organization |
|---|---|
| 1 | Princeton University<br>Princeton, New Jersey<br>Attn: Prof. D. Bershader |
| 1 | Pennsylvania State University<br>Physics Department<br>State College, Pennsylvania<br>Attn: Prof. R. G. Stoner |
| 1 | University of Michigan<br>Department of Physics<br>Ann Arbor, Michigan<br>Attn: Prof. Otto LaPorte |
| 4 | Institute for Fluid Dynamics and Applied Mathematics<br>University of Maryland<br>College Park, Maryland<br>Attn: A. Weinstein<br>S. I. Pai<br>R. Betchov<br>E. L. Resler, Jr. |
| 1 | University of California<br>Low Pressures Research Project<br>Berkeley, California<br>Attn: Prof. S. A. Schaaf |
| 1 | University of Illinois<br>Aeronautical Institute<br>Urbana, Illinois<br>Attn: Prof. C. H. Fletcher |
| 1 | University of Michigan<br>Aeronautical Research Center<br>Willow Run Airport<br>Ypsilanti, Michigan |
| 1 | United Aircraft Corporation<br>Research Department<br>East Hartford, Connecticut |
| 1 | Dr. A. E. Puckett<br>Hughes Aircraft Company<br>Florence Ave. at Teal St.<br>Culver City, California |
| 1 | Professor W. Bleakney<br>Palmer Physical Laboratory<br>Princeton University<br>Princeton, New Jersey |
| 2 | Professor J. O. Hirschfelder<br>Chemistry Department<br>University of Wisconsin<br>Madison 6, Wisconsin |
| 1 | Professor H. W. Emmons<br>Harvard University<br>Cambridge 38, Massachusetts |
| 1 | Professor L. S. G. Kovaszny<br>912 Belgian Avenue<br>Baltimore 18, Maryland |